This is a repository copy of *The Mechanics of Motorised Momentum Exchange Tethers when applied to Active Debris Removal from LEO*.

White Rose Research Online URL for this paper:
http://eprints.whiterose.ac.uk/118460/

Version: Published Version

Proceedings Paper:
Caldecott, R., Kamarulzaman, D.N.S., Kirrane, J.P. et al. (2 more authors) (2014) The Mechanics of Motorised Momentum Exchange Tethers when applied to Active Debris Removal from LEO. In: 10TH INTERNATIONAL CONFERENCE ON MATHEMATICAL PROBLEMS IN ENGINEERING, AEROSPACE AND SCIENCES (ICNPAA 2014). 10TH INTERNATIONAL CONFERENCE ON MATHEMATICAL PROBLEMS IN ENGINEERING, AEROSPACE AND SCIENCES: ICNPAA 2014, 15/07/2014 –18/07/2014, Narvik, Norway. AIP Conference Proceedings, 1637 . AIP Publishing , pp. 150-164. ISBN 978-0-7354-1276-7

https://doi.org/10.1063/1.4904574

Reuse
Unless indicated otherwise, fulltext items are protected by copyright with all rights reserved. The copyright exception in section 29 of the Copyright, Designs and Patents Act 1988 allows the making of a single copy solely for the purpose of non-commercial research or private study within the limits of fair dealing. The publisher or other rights-holder may allow further reproduction and re-use of this version - refer to the White Rose Research Online record for this item. Where records identify the publisher as the copyright holder, users can verify any specific terms of use on the publisher's website.

Takedown
If you consider content in White Rose Research Online to be in breach of UK law, please notify us by emailing eprints@whiterose.ac.uk including the URL of the record and the reason for the withdrawal request.

eprints@whiterose.ac.uk
https://eprints.whiterose.ac.uk/

The mechanics of motorised momentum exchange tethers when applied to active debris removal from LEO

Ralph Caldecott, Dayangku N. S. Kamarulzaman, James P. Kirrane, Matthew P. Cartmell, and Olga A. Ganilova

Citation: AIP Conference Proceedings **1637**, 150 (2014); doi: 10.1063/1.4904574
View online: http://dx.doi.org/10.1063/1.4904574
View Table of Contents: http://aip.scitation.org/toc/apc/1637/1
Published by the American Institute of Physics

The Mechanics of Motorised Momentum Exchange Tethers when applied to Active Debris Removal from LEO

Ralph Caldecott, Dayangku N.S. Kamarulzaman, James P. Kirrane, Matthew P. Cartmell and Olga A. Ganilova

Department of Mechanical Engineering, University of Sheffield, Mappin St., Sheffield, S1 3JD, England, UK

Abstract. The concept of momentum exchange when applied to space tethers for propulsion is well established, and a considerable body of literature now exists on the on-orbit modelling, the dynamics, and also the control of a large range of tether system applications. The authors consider here a new application for the Motorised Momentum Exchange Tether by highlighting three key stages of development leading to a conceptualisation that can subsequently be developed into a technology for Active Debris Removal. The paper starts with a study of the *on-orbit mechanics of a full sized motorised tether* in which it is shown that a laden and therefore highly mass-asymmetrical tether can still be forced to spin, and certainly to librate, thereby confirming its possible usefulness for active debris removal (ADR). The second part of the paper concentrates on the modelling of the *centripetal deployment* of a symmetrical MMET in order to get it initialized for debris removal operations, and the third and final part of the paper provides an entry into scale modelling for low cost mission design and testing. It is shown that the motorised momentum exchange tether offers a potential solution to the removal of large pieces of orbital debris, and that dynamic methodologies can be implemented to in order to optimise the emergent design.

1. INTRODUCTION

The symmetrical motorised momentum exchange tether is a specialisation of the momentum exchange tether and has been in continual development by the fourth author and others since 1996. Proposals for the on-orbit three dimensional dynamics of a dumb-bell version of this concept were first published in 1998 [1] and there have subsequently been several major studies carried out by students and collaborators of the fourth author since that time, with some selected relevant publications given in [2-12]. Current research activity is centred on interplanetary payload propulsion using motorised tethers [11, 12] and now on debris removal from LEO and the local vicinity. The active removal of space debris (ADR) is the focus of a major international research effort driven by the fact that the quantity of orbiting debris objects is increasing inexorably year on year, with around 19000 known objects having a principal dimension exceeding 5 cm and tracked by the US Space Surveillance Network. Around 95% of these objects constitutes some form of man-made or naturally sourced debris [13], but in fact most space debris is less than 1cm in size and is too small to be tracked. Collisions with debris of this size are unavoidable and so spacecraft are designed using debris shields to protect against the erosion inevitable with such contacts with the help of modern materials [14]. Large external components, particularly solar panels, are much harder to protect and so are often damaged. Anything over 10cm is definitely large enough to track and NASA has nearly completed cataloguing all objects in this category. If a collision trajectory is calculated to have a probability greater than 1 in 10000, a collision avoidance manoeuvre can be initiated to alter the course of the intercepting vehicle's orbit by increasing or decreasing its velocity. Debris objects that have a principal dimension greater than 10cm represent 0.5% of the debris population but 95% of the total mass [15]. Recent studies have confirmed that the current population can be stabilised by removing five large objects per year [16]. To place this in context other studies have shown that due to a critical density already having been reached, and even if all future space missions were to be halted, the space debris population would continue to increase due to collisions of objects already in orbit, creating a chain reaction. This phenomenon is now known as the *Kessler Syndrome*, as reported by Caldecott [17] The general tether literature is huge, but the

10th International Conference on Mathematical Problems in Engineering, Aerospace and Sciences
AIP Conf. Proc. 1637, 150-164 (2014); doi: 10.1063/1.4904574
© 2014 AIP Publishing LLC 978-0-7354-1276-7/$30.00

sub-set of papers dealing with externally excited, or motorised, tethers is relatively limited. The application of formal scaling theory to tether dynamics provides a basis for ensuring a useful form of dynamic similarity between scale models and full-size designs, and this approach was first explored by Cartmell and Ziegler [3] to investigate the further feasibility of the motorised momentum exchange tether. Further on-orbit analysis by Kamarulzaman [18] has recently revealed that certain provisos have to be satisfied in order to obtain practically useable results which can be applied to ADR scenarios. Practical tether applications in space all require some form of deployment of the tether from its supply module, and there are a limited number of possibilities for achieving this in practice. In all cases it is possible to deploy from the spool by means of active propulsion or ejection of the free end out from the supply module, but in the case of motorised tethers, which by definition librate or spin, then there is the additional option of some form of centripetal deployment. Centripetal deployment is examined in the last section of the paper and although this is not a new concept *per se*, and the general principles have been discussed in some detail by Danilin *et al* [19] and Levin [20], the modelling of a variable length motorised tether undergoing centripetal deployment is discussed for the first time by Kirrane [21]. In this paper we concentrate on developing a simple but useful precursor model for the application of a motorised momentum exchange tether to ADR and place that in the context of orbital modelling, and deployment from an as-delivered package on-orbit.

2. ACTIVE DEBRIS REMOVAL USING A MOTORISED MOMENTUM EXCHANGE TETHER

The first steps necessary in designing a tether-based mission for ADR are (i) to decide on scale, location, and associated tether dynamics for debris removal, then (ii) one needs to consider how the tether may be deployed and operated, and finally (iii) to decide if it would be feasible to do all the necessary research theoretically, or whether a test mission be needed, and if so, at what scale and cost. On the basis that all three criteria can be reasonably satisfied then specific design requirements can be identified, as follows:

To guarantee predictable dynamic performance – the tether always needs to be in the right place at the right time.

To provide fast error compensation through GNC with emergency on-board propulsion.

To minimise the use of emergency propellant.

To ensure robustness of performance, introducing a trade-off between redundancy and mass penalty.

To guarantee the highest possible reliability both at the component and the system levels.

To exploit fully motorised momentum exchange tether dynamics whereby missions can be configured to hang, librate, spin, or translate, or to utilise pre-determined mixed motions.

Finally if a low cost test mission is found to be necessary, to evaluate end-to-end performance and mission critical failure modes. All pertinent aspects of this need to be considered from the start of the design process.

The advantage of using a tether to interact with larger debris objects is that it can hang, librate, or spin, therefore it offers a lot of different dynamics to design around. It can also operate at virtually any altitude in LEO or MEO, with typical orbital velocities shown in Figure 1. A double-ended librating or spinning tether has particular potential because in principle it could clear a swathe of orbital space, as indicated in Figure 2.

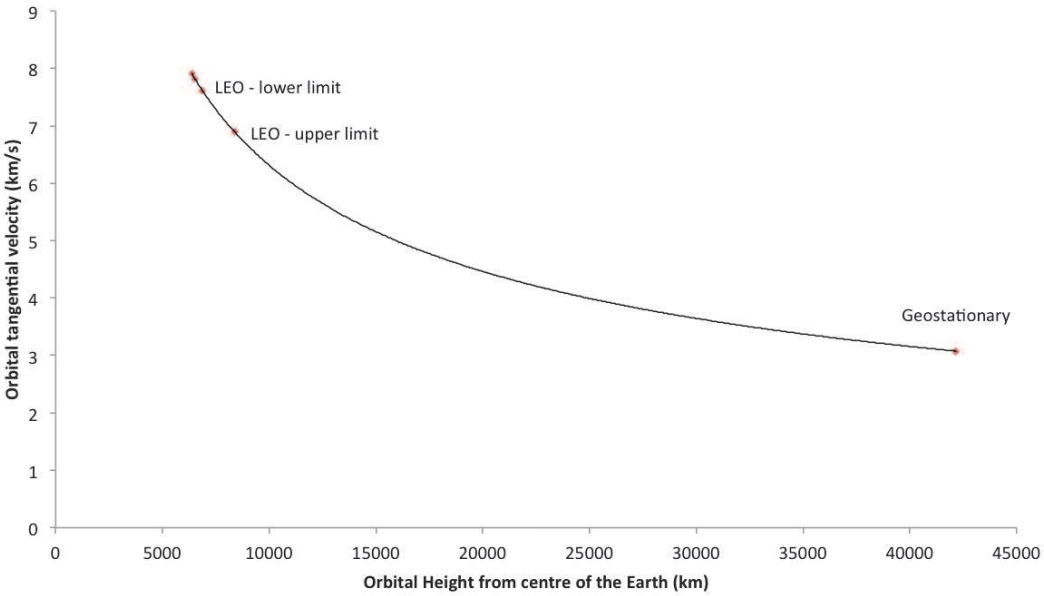

FIGURE 1. Orbital velocity with altitude.

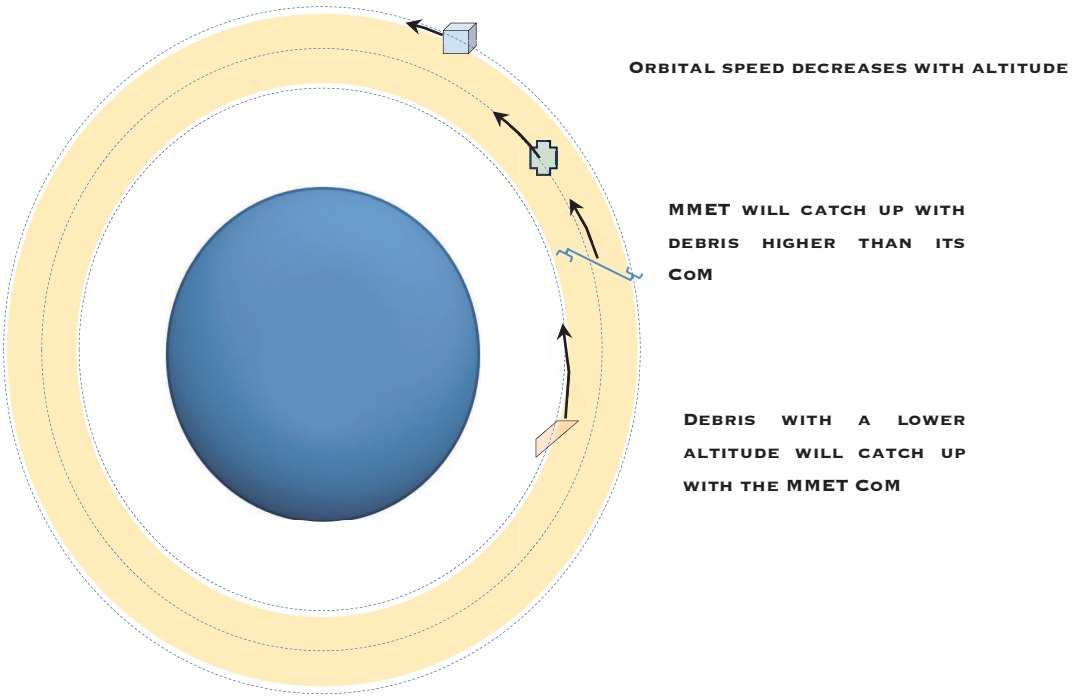

FIGURE 2. Principle of MMET application on orbit.

There will obviously be significant implications for dynamic performance due to the asymmetrical load distribution of debris on the system, and this is explored next in a preliminary model for the simplest case of a planar system on a circular Earth orbit, shown in Figure 3 for the case where the debris has been captured by an effector within the mass denoted by M_{p1}.

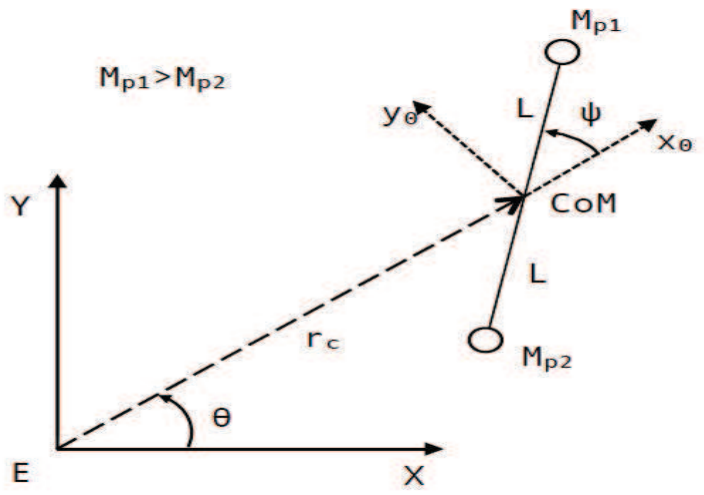

FIGURE 3. Planar tether on a circular Earth orbit

The objectives of the dynamic model are:

To devise a simple test architecture for a spinning motorised tether on a circular orbit for debris collection.

To couple this to rigid body tether dynamics for an initial scoping analysis.

Finally to employ a double-ended dumb-bell tether with asymmetrical mass distribution due to loading with large pieces of debris.

Certain simplifying assumptions are made by which a tractable and relatively simple model can be conjectured which will also possess some realism, as depicted In Figure 3:

A planar system can be assumed on a circular Earth orbit.

M_{p1} represents both a catcher/end effector and a substantial piece of debris.

M_{p2} could be another catcher and piece of debris, or just a counter-mass.

The debris attaches to M_{p1} with negligible shock load.

The debris velocity vector is close to that of the tangential component at M_{p1}.

The Cartesian components implicit in Figure 3 can readily be converted into polar coordinates, as follows,

$$\begin{aligned} x_{p1} &= r_c cos\theta + Lcos(\theta+\psi) & y_{p1} &= r_c sin\theta + Lsin(\theta+\psi) \\ x_{p2} &= r_c cos\theta - Lcos(\theta+\psi) & y_{p2} &= r_c sin\theta - Lsin(\theta+\psi) \\ & & x_m &= r_c cos\theta \\ & & y_m &= r_c sin\theta \end{aligned} \qquad (1)\text{-}(10)$$

$$\begin{aligned} x_{T1} &= r_c cos\theta + \frac{L}{2}\cos(\theta+\psi) & x_{T2} &= r_c cos\theta - \frac{L}{2}\cos(\theta+\psi) \\ y_{T1} &= r_c sin\theta + \frac{L}{2}sin(\theta+\psi) & y_{T2} &= r_c sin\theta - \frac{L}{2}sin(\theta+\psi) \end{aligned}$$

from which the rotational kinetic energy can be constructed,

$$T = \frac{1}{2}M_{p1}(\dot{x}_{p1}^2+\dot{y}_{p1}^2) + \frac{1}{2}M_{p2}(\dot{x}_{p2}^2+\dot{y}_{p2}^2) + \frac{1}{2}M_m(\dot{x}_m^2+\dot{y}_m^2) + \frac{1}{2}\rho Al(\dot{x}_{t1}^2+\dot{y}_{t1}^2) + \frac{1}{2}\rho Al(\dot{x}_{t2}^2+\dot{y}_{t2}^2) + \underbrace{\left\{\frac{1}{2}(2I_p+2I_t+I_m)(\dot{\theta}+\dot{\psi})^2\right\}}_{Kinetic\ Energy\ due\ to\ Rotation} \qquad (11)$$

noting that care must be taken in constructing the mass moment of inertia terms for the asymmetrical mass distribution cases. The system potential energies can also be obtained from Newton's universal

theory of gravitation and the physical orientation of the principal parts of the system shown in Figure 3. The potential energies of the payloads, main facility, and tether sub-spans are all given as follows,

$$U_{P1} = -\frac{\mu M_{P1}}{\sqrt{r_c^2 + L^2 + 2r_c L cos\psi}} \qquad U_{P2} = -\frac{\mu M_{P2}}{\sqrt{r_c^2 + L^2 - 2r_c L cos\psi}}$$

$$U_m = -\frac{\mu M_m}{r_c} \tag{12-16}$$

$$U_{T1} = -\mu\rho A \int_0^l (r_c^2 + z^2 + 2r_c z cos\psi)^{-\frac{1}{2}} dz = \mu\rho A ln \frac{r_c(1 + cos\psi)}{L + r_c cos\psi + \sqrt{r_c^2 + L^2 + 2r_c L cos\psi}}$$

$$U_{T2} = -\mu\rho A \int_0^l (r_c^2 + z^2 + 2r_c z cos\psi)^{-\frac{1}{2}} dz = \mu\rho A ln \frac{r_c(1 - cos\psi)}{l - r_c cos\psi + \sqrt{r_c^2 + L^2 - 2r_c L cos\psi}}$$

Lagrange's Equation is used to derive the equation of motion, and a generalised force is inserted to excite directly the generalised coordinate ψ. This second order ODE is more complicated than the usual mass-symmetrical system for which $M_{p1} = M_{p2}$, and is generated automatically in *Mathematica*. Note that the the simpler symmetrical version is used in the two subsequent sections of the paper. The numerical data used is given in the following vector,

$$\{L, M_{p_1}, M_{p_2}, \rho, A, M_m, r_m, r_{p_1}, r_{p_2}, r_c, \mu, \tau\}$$
$$= \{50000,1200,1200,970,62.83 * 10^{-6}, 5000,0.5,0.5,0.5,6870000,3.9877848$$
$$* 10\text{^}14,25000000\}$$

and this is generally consistent with other studies [1-7]. The most important point here is that the second and third entries in the vector, M_{p1} and M_{p2} , can be varied in order to explore the degree of mass asymmetry. This phenomenon is summarised in Figure 4, in which the degree of mass asymmetry increases towards the abscissa, with an extreme case given (316.7%) in which spin is quenched in favour of libration (astronomical oscillation). This is shown in detail in Figure 5.

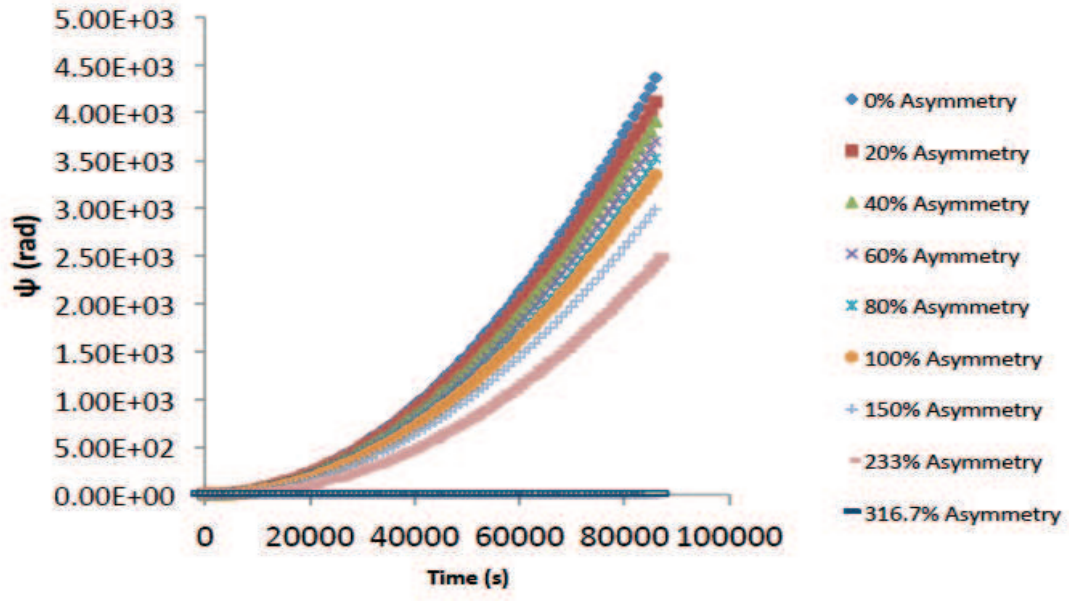

FIGURE 4. Tether spin angle with time for varying mass asymmetries.

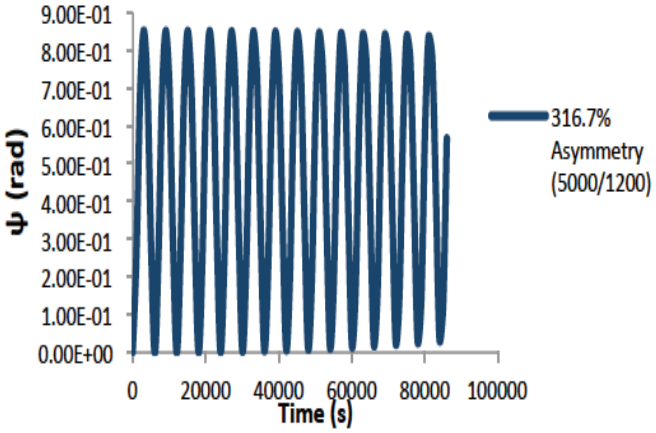

FIGURE 5. The case for 316.7% mass asymmetry.

Figure 6 offers an insight into the relationships between tether spin angle and angular velocity with time, for torque switch-off at 4000 seconds. This calculation suggests a simple methodology for implementing a choice of spin rate prior to engagement with the debris.

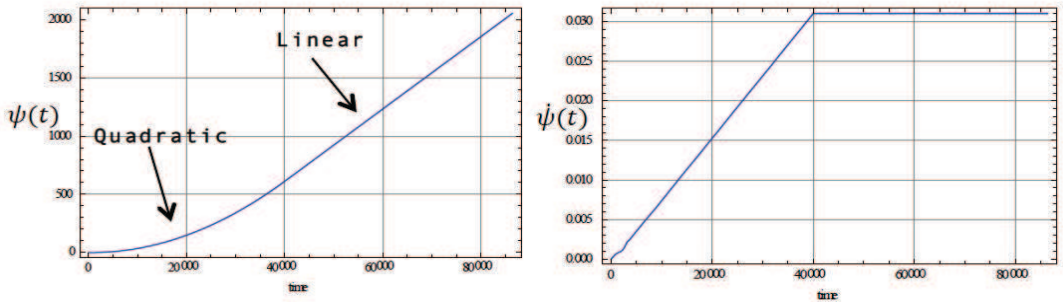

FIGURE 6. Tether angular displacement and velocity, with time.

Figure 7 shows the effect of intercepting a piece of debris of 2800 kg (equivalent to a mass asymmetry of 233%) at three arbitrarily chosen times and confirms that although the tether's angular acceleration at each interception point changes, the later the interception the less significant the reduction in angular acceleration turns out to be.

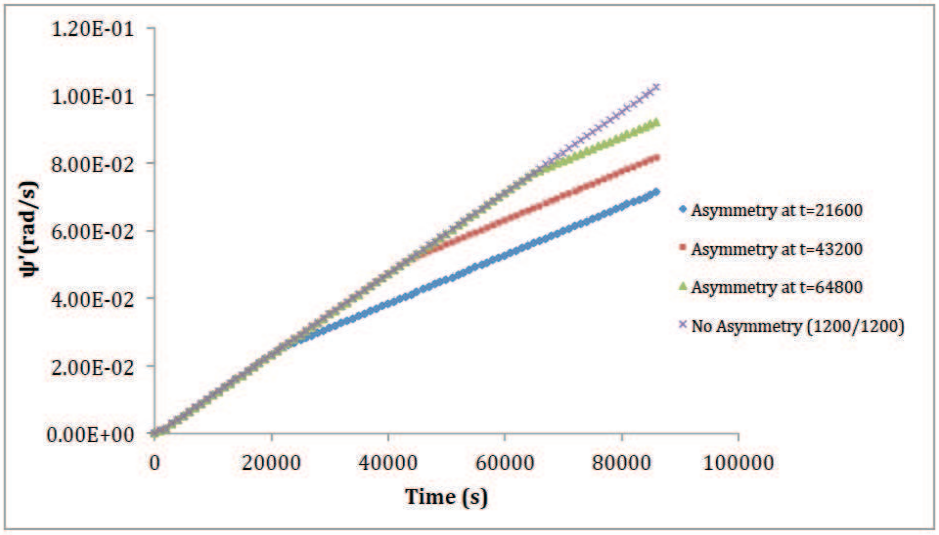

FIGURE 7. The effect on angular velocity of intercepting a large piece of debris of mass 2800 kg (such that M_{p1} goes from 1200 to 4000 kg, a mass asymmetry of 233%) at specific times.

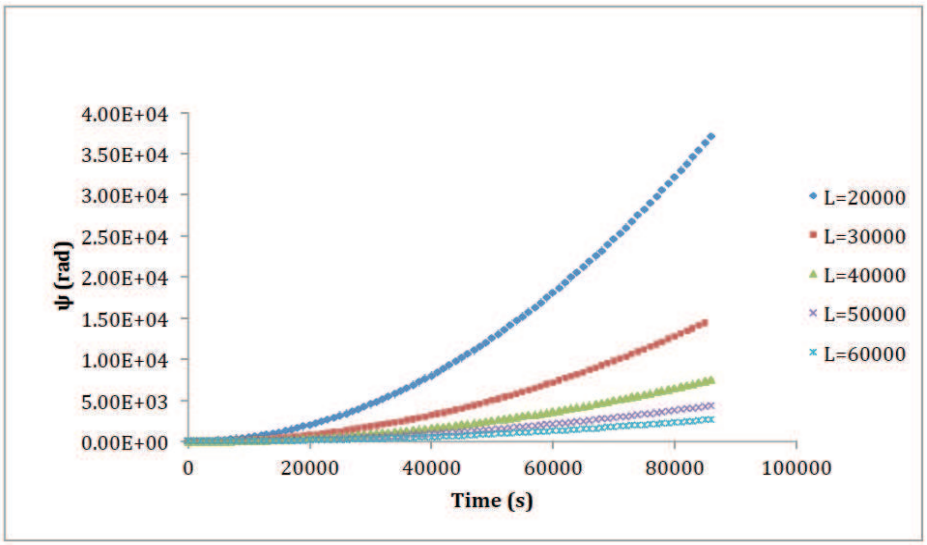

FIGURE 8. The change in angular displacement with time for a symmetrical tether for different sub-span lengths.

Another important relationship is given in Figure 8 where the response of a mass-symmetrical system is presented against time for a range of different sub-span lengths, thus confirming that longer systems accelerate more slowly than their shorter counterparts. This relatively obvious conclusion is further examined in the deployment context in the next section.

In order to design an end effector for a tether that can collect debris reliably there are three principal design requirements which must be met:

1. The capture device should have as low a mass as possible consistent with sufficient structural rigidity.
2. It should be versatile enough to capture a wide range of debris geometries.
3. It should be capable of securing the debris upon capture and remain secure until the point of release whereupon the debris should not be able to be caught unintentionally in the rest of the system.

A popular conceptual solution for debris collector design is a net-like device which can open and then close around the debris at the right time, and which can wrap and conform around objects of varying shapes and sizes. The principal feature of all debris is that it is uncooperative, with largely unknown dynamics at the point if interception. A net-based sweeper/collector system fitted to a momentum exchange tether could work in the following manner:

- The debris target is known to be in range and the tether is rotating towards it.
- The sweeper/collector net is opened sufficiently to surround the debris.
- The interception is at the lowest relative velocity possible and the net is closed to secure the debris.
- The tether is accelerated or at the least rotated at constant velocity until the ideal point of release is attained. At this point the net is opened and the tether is decelerated in order to slow it down relative to the debris which can then be released tangentially and into a new orbit.

The bi-stable thermal state of a shape memory alloy could be used in the design of a net sweeper/collector, using pumped liquid ammonia running in conductive tubes alongside the active shape memory alloy elements of the net, as shown in Figure 9. The liquid ammonia has two functions, one being to provide a source of heat conduction to and from the SMAs and the other to assist the SMA in manipulating the overall shape of the net sweeper/collector. A preliminary design of such a system has been undertaken [17] and is shown in schematic form in Figures 9 and 10.

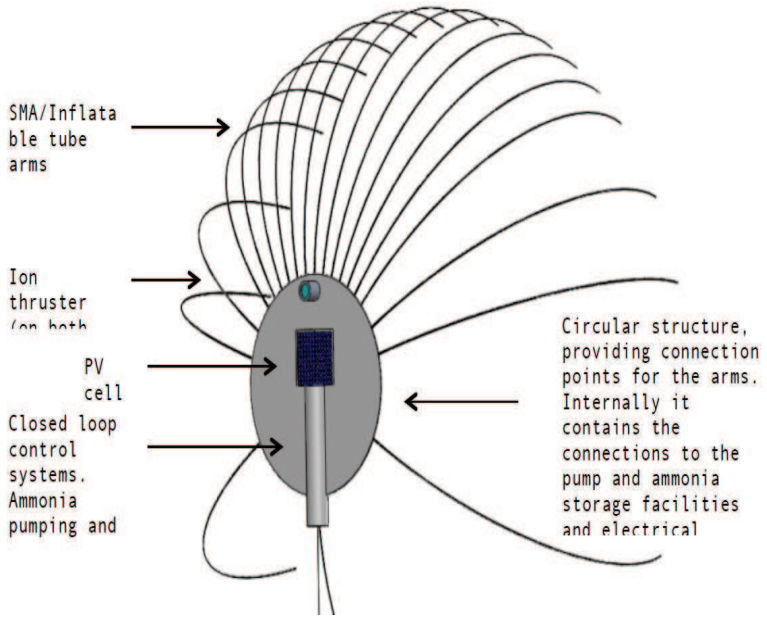

FIGURE 9. Debris capture concept showing the sweeper in the open configuration.

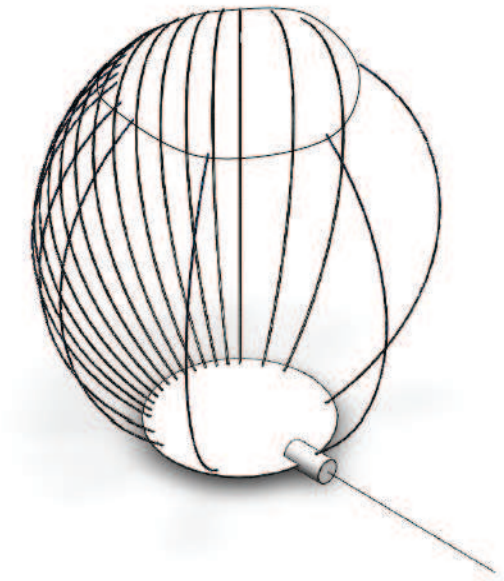

FIGURE 10. Debris capture concept showing the sweeper in the closed configuration.

To summarise, a motorised momentum exchange tether could be configured to clear large pieces of debris, one by one, by interacting with a chaser capture device in the form of a net-like sweeper/collector fitted at the end of a tether sub-span. Such a system could potentially clear a ring shaped swathe of space, with dimensions defined by the tether's altitude and the end-to-end length. It could also be configured to sweep up clouds of small debris in similar regions by means of a finer net. The success of such a system in practice will depend not only on the above operations but also on initialising the tether system into location and getting it ready to go. It will also need the capability of being reset after use so that new dynamic conditions can be met as necessary. This requires a reliable and controllable form of sub-span deployment and in all probability the design of a low-cost scale model test mission to evaluate a trial technology.

3. DEPLOYMENT STUDY

Motorised tethers can undertake three discrete motions which are all of direct use, plus any amount of intermediate and mixed-mode motions, with the most complex bifurcatory behaviour evident in those cases. The assumption here is to assume a pre-deployment package which is delivered to the appropriate location in LEO and then deployed in a controllable and predictable manner. There are two obvious conceptual solutions to this problem:

- to deploy passive sub-spans by using payload thrusters to pull the system into deployment,
- to use centripetal deployment through system spin-up from the delivery configuration to full deployment.

Whilst the first solution is relatively simple it requires active payloads and additional propellant on board, with obvious cost and mass implications. The second solution simply exploits the dynamics of the spin-up inherent to the system and is therefore preferable. In order to examine the potential for centripetal deployment we assume the following data:
$l_{1(\mathrm{dep})}$ = 25 km, r_{To} = 0.006 m, r_{Ti} = 0.004 m, ρ = 970 kg/m^3, $M_{\mathrm{T1}} = M_{\mathrm{T2}} = M_{\mathrm{T}} = \rho\pi(r_{To}^2 - r_{Ti}^2)l_{1(dep)}$ = 1523.6 kg, M_{M} = 8047.2 – 2(1523.6) = 5000 kg, $M_{\mathrm{p1}} = M_{\mathrm{p2}} = M_{\mathrm{p}}$ = 1000 kg, $r_{\mathrm{m}} = r_{\mathrm{p}}$ = 0.5 m, h_{m} = 5m, h_{p} = 1m.

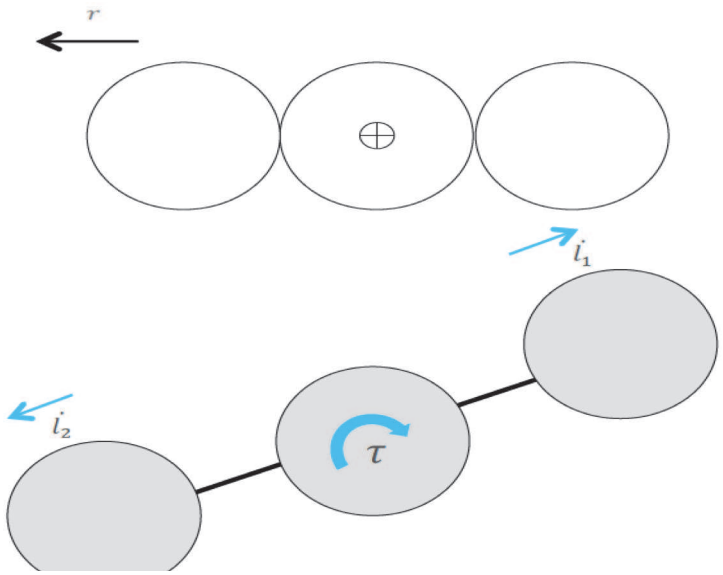

FIGURE 11. Conceptual solutions for thrust (top) and centripetal deployers (bottom).

The planar tether model is taken here as in the ADR reference study in section 2 however it is restricted to a system with mass-symmetry here in order to avoid confusion between the dynamic effects of mass asymmetry and centripetal deployment. This approach will also provide a basis for identical deployment dynamics for each sub-span. The generalised coordinates for the model are ψ, l_1, and l_2. The three equations of motion are derived using a Lagrangian derivation similar to that of section 1, and emerge in the following forms, noting that damping of the form $B\dot{l}_1$ and $B\dot{l}_2$ is subsequently added into the equations in l_1 and l_2, respectively, in order to get the numerical results presented below in Figures 12 and 13.

$$\left(M_p {r_p}^2 + M_p\left({l_1}^2 + {l_2}^2\right) + \frac{(M_{T1} + M_{T2}){r_T}^2}{4} + \frac{M_T\left({l_1}^2 + {l_2}^2\right)}{3} + \left(\frac{M_{m0}}{2} - M_T\right){r_m}^2\right)\ddot{\psi}$$
$$+ 2M_p\left(\dot{l_1}l_1 + \dot{l_2}l_2\right)\left(\dot{\theta} + \dot{\psi}\right) + \left(M_{T1}\dot{l_1}l_1 + M_{T2}\dot{l_2}l_2\right)\left(\dot{\theta} + \dot{\psi}\right)$$
$$+ \left(\frac{{r_T}^2}{4} - \frac{{r_m}^2}{2}\right)A\rho\left(\dot{l_1} + \dot{l_2}\right)\left(\dot{\theta} + \dot{\psi}\right)$$
$$+ \mu\left(-\frac{M_p r_c l_1 sin(\psi)}{\sqrt{\left({r_c}^2 + 2cos(\psi)r_c l_1 + {l_1}^2\right)^3}} + \frac{M_p r_c l_2 sin(\psi)}{\sqrt{\left({r_c}^2 - 2cos(\psi)r_c l_2 + {l_2}^2\right)^3}}\right.$$
$$\left. - \frac{4M_T r_c l_1 sin(\psi)}{\sqrt{\left(4{r_c}^2 + 4cos(\psi)r_c l_1 + {l_1}^2\right)^3}} + \frac{4M_T r_c l_2 sin(\psi)}{\sqrt{\left(4{r_c}^2 - 4cos(\psi)r_c l_2 + {l_2}^2\right)^3}}\right)$$
$$+ \left(M_p r_c sin(\psi)\dot{\theta}^2 + \frac{A\rho r_c \sin(\psi)\dot{\theta}^2}{2}\right)\left({l_1}^2 - {l_2}^2\right)$$
$$+ \frac{A\rho r_c \cos(\psi)\dot{\theta}}{2}\left(\dot{l_1}l_1 - \dot{l_2}l_2\right) = Q_\psi \tag{17}$$

$$\left(M_p + \frac{M_{T1}}{4}\right)\ddot{l_1} - \left(M_p + M_{T1}\right)r_c\dot{\theta}^2 cos(\psi) + \left(-M_p l_1 - \frac{M_{T1}l_1}{2} - \frac{A\rho {r_T}^2}{8} + \frac{A\rho {r_m}^2}{4}\right)\left(\dot{\theta} + \dot{\psi}\right)^2$$
$$- \frac{M_{T1}r_c\dot{\theta}\dot{\psi}cos(\psi)}{2}$$
$$+ \mu\left(\frac{M_p(r_c\cos(\psi) + l_1)}{\sqrt{\left({r_c}^2 + 2cos(\psi)r_c l_1 + {l_1}^2\right)^3}} - \frac{4A\rho r_c\left(2r_c + l_1 cos(\psi)\right)}{\sqrt{\left(4{r_c}^2 + 4cos(\psi)r_c l_1 + {l_1}^2\right)^3}} + \frac{A\rho}{r_c}\right)$$
$$+ \frac{1}{8}A\rho\dot{l_1}^2 = Q_{l_1} \tag{18}$$

$$\left(M_p + \frac{M_{T2}}{4}\right)\ddot{l_2} + \left(M_p + M_{T2}\right)r_c\dot{\theta}^2 cos(\psi) + \left(-M_p l_2 - \frac{M_{T2}l_2}{2} - \frac{A\rho {r_T}^2}{8} + \frac{A\rho {r_m}^2}{4}\right)\left(\dot{\theta} + \dot{\psi}\right)^2$$
$$+ \frac{M_{T2}r_c\dot{\theta}\dot{\psi}cos(\psi)}{2}$$
$$+ \mu\left(-\frac{M_p(r_c cos(\psi) - l_2)}{\left({r_c}^2 - 2cos(\psi)r_c l_2 + {l_2}^2\right)^{\frac{3}{2}}} - \frac{4A\rho r_c\left(2r_c - l_2 cos(\psi)\right)}{\left(4{r_c}^2 - 4cos(\psi)r_c l_2 + {l_2}^2\right)^{\frac{3}{2}}} + \frac{A\rho}{r_c}\right)$$
$$+ \frac{1}{8}A\rho\dot{l_2}^2 = Q_{l_2} \tag{19}$$

Numerical integration of equations (17)-(19) is undertaken using *Mathematica* and the damped deployer response from zero is obtained for $\tau = Q_\psi = 25$ kNm, $Q_{l1} = Q_{l2} = 0$, $B = 250$ kg/s, and deployment stopped by a brake at $t = 1870$ to 1910 s. The responses of l_1 and l_2 are shown respectively in Figures 12(a) and 12(b).

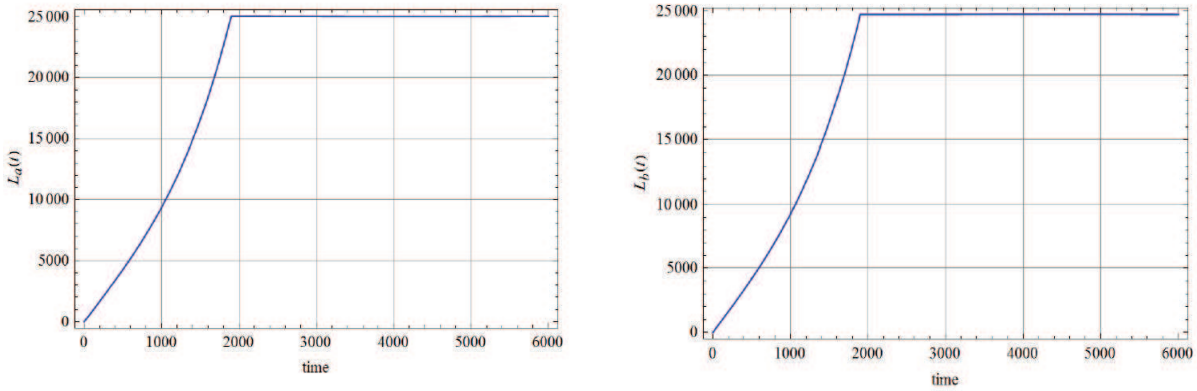

FIGURE 12. (a) Damped and braked deployer response for l_1, (b) Damped and braked deployer response for l_2.

Smooth and well controlled deployment is evident for both sub-spans in Figures 12(a) and 12(b), with a brake actuated during the interval of 1870 to 1910 s. Many other deployment characteristics can be identified for this system but it is considered that the profiles shown here are indicative of a desirable deployment function.

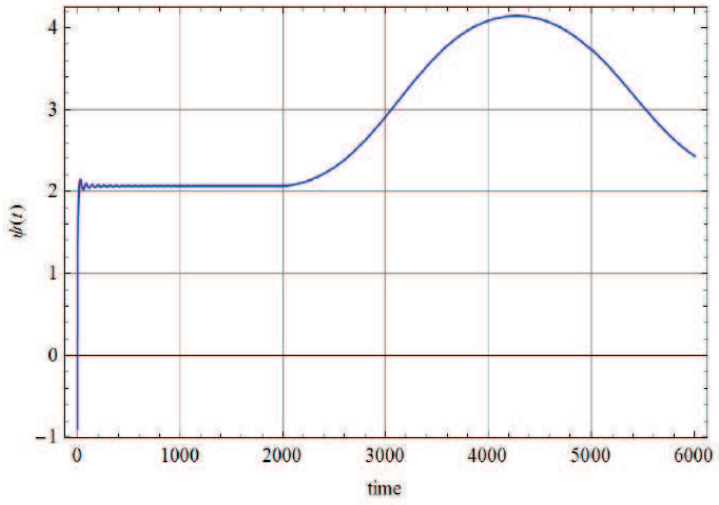

FIGURE 13. Corresponding response of ψ against time.

Figure 13 shows the response of the system in ψ where a small amplitude libration is evident about a 2 radian offset during deployment until braking starts, and then a large swing and subsequent return to small angle libration about the offset of 2 radians, at around 6000 s. Clearly once the two sub-spans are fully deployed then the deployer can be locked, effectively returning the system to a single degree of freedom model with freedom to revert to any chosen form of motion after around 2000s. Sub-span velocity responses during the braking phase are shown in Figures 14(a) and 14(b).

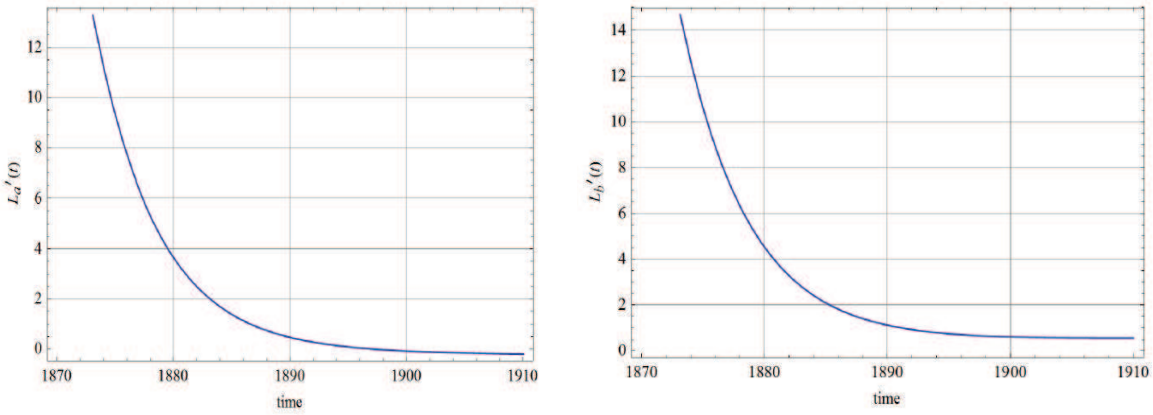

(a) (b)

FIGURE 14. (a) Time response of the sub-span velocity, $\dot{l}_1$, (b) Time response of the sub-span velocity, $\dot{l}_2$.

It should be noted that in practice braking would require a precisely controllable deployer brake such as the 'barberpole' concept [8]. A torque in the order of MNm is required to spin the tether system up but it has been shown in this study that deployment of the sub-spans can in fact be ensured by torques even in the kNm region.

4. SCALE MODELLING

The ADR reference and deployment studies summarised in sections 2 and 3 of this paper are both greatly simplified yet represent some of the fundamentally important dynamic features of such a system. An experimental test campaign will be required to demonstrate the validity and robustness of those dynamic features on-orbit. In order to accomplish this a scale modelling analysis is required. Some preliminary work has been carried out based on the same level of modelling, and a single line motorised planar tether is modelled on a circular Earth orbit. For which the equation of motion is as follows,

$$\left(\frac{M_m r_m^2}{2} + M_p\left(2l^2 + r_p^2\right) + \frac{\rho A l[4l^2 + 3r_T^2]}{6}\right)\ddot{\Psi} + \frac{\mu M_p r_c l \sin\Psi}{(r_c^2 + l^2 - 2r_c l\cos\Psi)^{3/2}} - \frac{\mu M_p r_c l \sin\Psi}{(r_c^2 + l^2 + 2r_c l\cos\Psi)^{3/2}} - \mu\rho A\frac{r_c^2 + l^2 - r_c l(1-\cos\Psi) + (l - r_c)\sqrt{r_c^2 + l^2 + 2r_c l\cos\Psi}}{r_c^2 + l^2 + 2r_c l\cos\Psi + (l + r_c\cos\Psi)\sqrt{r_c^2 + l^2 + 2r_c l\cos\Psi}}\tan\left(\frac{\Psi}{2}\right) + \mu\rho A\frac{r_c^2 + l^2 - r_c l(1+\cos\Psi) + (l - r_c)\sqrt{r_c^2 + l^2 - 2r_c l\cos\Psi}}{r_c^2 + l^2 - 2r_c l\cos\Psi + (l + r_c\cos\Psi)\sqrt{r_c^2 + l^2 - 2r_c l\cos\Psi}}\cot\left(\frac{\Psi}{2}\right) = \tau \tag{20}$$

Vaschy-Buckingham-Langhaar scaling theory is used to synthesise a scale model from a full-size model, or vice versa by means of dimensionless pi-terms. All the dimensional quantities within the model are entered into a vector,

$$\{P\} = [\mu, \rho, \tau, A, l, M_m, M_p, r_c, r_m, r_p, r_T, t]^T \tag{21}$$

from which an equation of dimensional homogeneity can be constructed in the *MLT* system,

$$\mu^{a_1}\rho^{a_2}\tau^{a_3}A^{a_4}l^{a_5}M_m^{a_6}M_p^{a_7}r_c^{a_8}r_m^{a_9}r_p^{a_{10}}r_T^{a_{11}}t^{a_{12}} = M^0L^0T^0 \tag{22}$$

Substitution of the appropriate dimensions and rearrangement leads to an identification of the dimensionless pi-terms, as follows,

$$\left(\frac{\mu t^2}{l^3}\right)^{a_1}\left(\frac{\rho l^5}{\tau t^2}\right)^{a_2}\left(\frac{A}{l^2}\right)^{a_4}\left(\frac{l^2 M_m}{\tau t^2}\right)^{a_6}\left(\frac{l^2 M_p}{\tau t^2}\right)^{a_7}\left(\frac{r_c}{l}\right)^{a_8}\left(\frac{r_m}{l}\right)^{a_9}\left(\frac{r_p}{l}\right)^{a_{10}}\left(\frac{r_T}{l}\right)^{a_{11}} = M^0 L^0 T^0 \tag{23}$$

Taking the first term as an example we can now create an appropriate scaling for it,

$$\frac{\mu_S t_S^2}{l_S^3} = \frac{\mu_F t_F^2}{l_F^3} \tag{24}$$

which leads to,

$$\frac{\mu_S}{\mu_F}\frac{t_S^2}{t_F^2} = \frac{l_S^3}{l_F^3} \tag{25}$$

from which a relationship between the Lambda scaling terms is derived,

$$\lambda_\mu \lambda_t^2 = \lambda_l^3 \tag{26}$$

This can also be accomplished for the other eight pi-terms,

$$\begin{gathered}
\lambda_l^5 \lambda_\rho = \lambda_\tau \lambda_t^2 \\
\lambda_A = \lambda_l^2 \\
\lambda_l^2 \lambda_{M_m} = \lambda_\tau \lambda_t^2 \\
\lambda_l^2 \lambda_{M_p} = \lambda_\tau \lambda_t^2 \\
\lambda_{r_c} = \lambda_l \\
\lambda_{r_m} = \lambda_l \\
\lambda_{r_p} = \lambda_l \\
\lambda_{r_T} = \lambda_l
\end{gathered} \tag{27-34}$$

Insertion of the Lambda pi-terms converts the original ODE of equation (20) into a scaled form for which dynamic similarity is assured,

$$\begin{aligned}
&\left(\frac{\lambda_\tau \lambda_t^2}{\lambda_{M_m}\lambda_l^2}\frac{M_{m_S} r_{m_S}^2}{2} + \frac{\lambda_\tau \lambda_t^2}{\lambda_{M_p}\lambda_l^2} M_{p_S}\left(2l_S^2 + r_{p_S}^2\right) + \frac{\lambda_\tau \lambda_t^2}{\lambda_\rho \lambda_l^5}\rho_S A_S l_S \frac{\left[4l_S^2 + 3r_{T_S}^2\right]}{6}\right)\ddot{\psi}_S \\
&+ \frac{\lambda_\tau \lambda_t^2}{\lambda_{M_p}\lambda_l^2}\frac{\mu M_{p_S} r_{c_F} l_S \sin\psi}{\left(r_{c_S}^2 + l_S^2 - 2r_{c_S} l_S \cos\psi\right)^{3/2}} - \frac{\lambda_\tau \lambda_t^2}{\lambda_{M_p}\lambda_l^2}\frac{\mu M_{p_S} r_{c_S} l_S \sin\psi}{\left(r_{c_S}^2 + l_S^2 + 2r_{c_F} l_S \cos\psi\right)^{3/2}} \\
&- \frac{\lambda_\tau \lambda_t^2}{\lambda_\rho \lambda_l^5}\mu \rho_S A_S \frac{r_{c_S}^2 + l_S^2 - r_{c_S} l_S\left(1 - \cos\psi\right) + \left(l_S - r_{c_S}\right)\sqrt{r_{c_S}^2 + l_S^2 + 2r_{c_S} l_S \cos\psi}}{r_{c_S}^2 + l_S^2 + 2r_{c_S} l_S \cos\psi + \left(l_S + r_{c_S}\cos\psi\right)\sqrt{r_{c_S}^2 + l_F^2 + 2r_{c_S} l_S \cos\psi}}\tan\left(\frac{\psi}{2}\right) \\
&+ \frac{\lambda_\tau \lambda_t^2}{\lambda_\rho \lambda_l^5}\mu \rho_S A_S \frac{r_{c_S}^2 + l_S^2 - r_{c_S} l_S\left(1 + \cos\psi\right) + \left(l_S - r_{c_S}\right)\sqrt{r_{c_F}^2 + l_F^2 - 2r_{c_F} l_F \cos\psi}}{r_{c_S}^2 + l_S^2 - 2r_{c_S} l_S \cos\psi + \left(l_S - r_{c_S}\cos\psi\right)\sqrt{r_{c_S}^2 + l_S^2 - 2r_{c_S} l_S \cos\psi}}\cot\left(\frac{\psi}{2}\right) = \tau_S
\end{aligned} \tag{35}$$

On the basis that the principal scaling is of the tether sub-span length then a 25000:1 length-scale model can be synthesised. This is based on identical geometries for the end effectors and central facility, and a *Spectra2000* tether of the same diameter as the full-size system, but with 250:1 scaling in the principal masses. The spin angle and spin angular velocity responses emerge as shown in Figures 15 and 16 for the data used here.

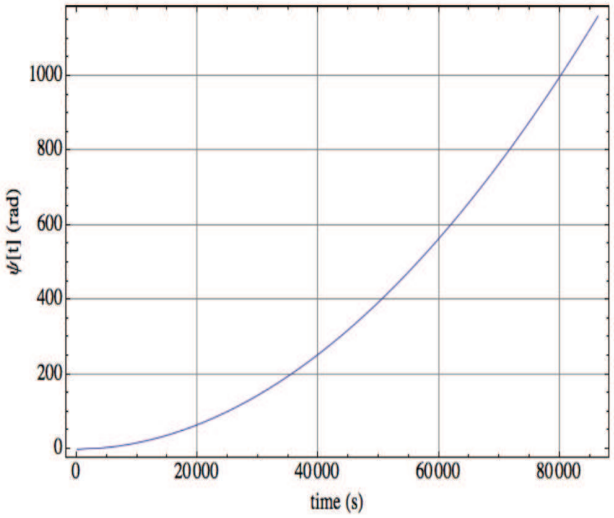

FIGURE 15. Spin angle response with time for the scale model.

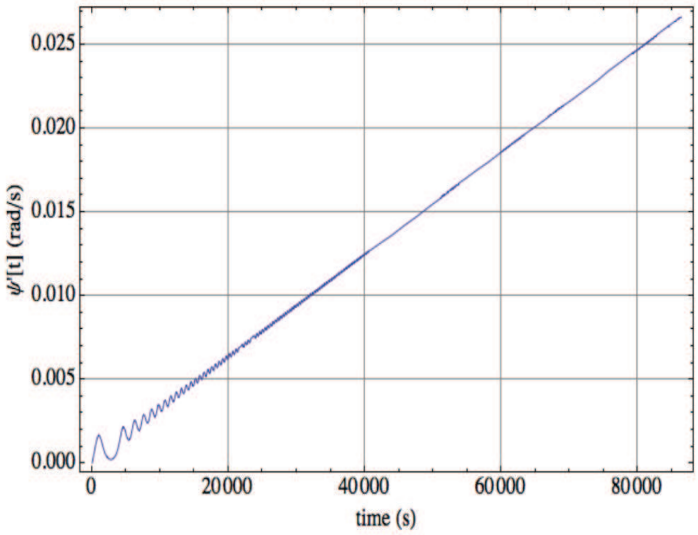

FIGURE 16. Spin angular velocity response with time for the scale model.

The results shown in Figures 15 and 16 are for one of a number of possible scaling scenarios and show that a scale model can be reliably used for dynamic prediction on-orbit of a full size motorised momentum exchange system, provided certain requirements are met. In particular that the tether diameter does not become vanishingly small on scaling. The drive torque for the scale model scales according to the appropriate pi-terms given in equations (27), (29), or (30). This result indicates that it should also be possible to scale more complicated orbital models incorporating non-circular and non-equatorial orbits, and models which also cater for tether flexure effects.

5. CONCLUSIONS

- Motorised tethers potentially offer clean, green, reusable propulsion in space. All likely orbits could in principle be accommodated.
- The dynamics of space tethers are complicated, and so robust GNC will be required in all practical mission scenarios.
- The application to ADR is very promising, with great potential for low-cost missions.
- Centripetal deployment during libration is a reliable, energy efficient, and controllable way of obtaining full sub-span extension.

- Assuming certain design trade-offs the preliminary scale modelling work suggests that low cost scale models could be tested on orbit to predict the corresponding performance of full size systems, and that an application of the scaling approach outlined here to an ADR scenario is entirely feasible.

ACKNOWLEDGEMENTS

The computational facilities provided by the University of Sheffield are gratefully acknowledged.

REFERENCES

1. M. P. Cartmell, "Generating Velocity Increments by Means of a Spinning Motorised Tether", in *34th AIAA/ASME/SAE/ASEE Joint Propulsion Conference and Exhibition*, Conference Proceedings, (Cleveland Conference Center, Cleveland, Ohio, USA, 3-15 July 1998), AIAA 98-3739
2. M. P. Cartmell, S. W. Ziegler, "Symmetrically Laden Motorised Tethers for Continuous Two-way Interplanetary Payload Exchange", in *35th AIAA/ASME/SAE/ASEE Joint Propulsion Conference and Exhibit*, Conference Proceedings, (Los Angeles, California, USA, 20-24, June 1999), AIAA 99-2840.
3. M. P. Cartmell, S. W. Ziegler, "Terrestrial Scale Model Testing of a Motorised Propulsion Tether", in *36th AIAA/ASME/SAE/ASEE Joint Propulsion Conference and Exhibit*, Conference Proceedings, (Huntsville, Alabama, USA, July 2000), AIAA 2000-3612.
4. S. W. Ziegler, M. P. Cartmell, "Investigating the Use of Motorised Tethers for Payload Orbital Transfer", in *AIAA/AAS Astrodynamics Specialist Conference and Exhibit*, Conference Proceedings, (Denver, Colorado, USA, 14-17 August 2000), AIAA 2000-4529.
5. S. W. Ziegler, M. P. Cartmell, "On the Validity of Recent Predictions for Tethers on Elliptical Orbits", in *11th AAS/AIAA Space Flight Mechanics Meeting*, Conference Proceedings, (Santa Barbara, California, USA, 11-15 February 2001), AAS01-233.
6. S.W. Ziegler and M. P. Cartmell, *AIAA Journal of Spacecraft and Rockets* **38 (6),** 904-913 (2001).
7. M. P. Cartmell, S. W. Ziegler, "Experimental Scale Model Testing of a Motorised Momentum Exchange Propulsion Tether", in *37th AIAA/ASME/SEA/ASEE Joint Propulsion Conference and Exhibition*, Conference Proceedings, (Salt Lake City, Utah, USA, 8-11 July 2001), AIAA 2001-3914.
8. S. Lennert, M. P. Cartmell, "Analysis and Design of a Friction Brake for Momentum Exchange Propulsion Tethers", in *Fifth IAA International Conference on Low-Cost Planetary Missions ESA/ESTEC*, Conference Proceedings, (September 2003).
9. D. J. McKenzie, M. P. Cartmell, Modelling of Tethered Space-Web Structures, in *56th IAC 2005*, Conference Proceedings, IAC-06-D4.3.07.
10. M. P. Cartmell and D. J. McKenzie, Progress in Aerospace Sciences **44 (1)**, 1-21 (2008).
11. C. Murray and M. P. Cartmell, Journal of Space Technology and Science (Special issue on Space Tethers and Elevators) **26 (1)**, 57 – 68 (2012).
12. C. Murray and M. P. Cartmell, Journal of Guidance, Dynamics, and Control **36**, 567-576 (2013).
13. J. C. Liou, N. L. Johnson and N. M. Hill, Acta Astronautica **66 (5-6)**, 648-653 (2010).
14. E.L. Christiansen, "Meteoroid/Debris Shielding, report NASA Johnson Space Centre", 2003.
15. National Research Council, *Orbital Debris*: *A Technical Assessment* (Washington DC, The National Academies Press), 1995.
16. M. M. Castronuovo, Acta Astronautica, **69 (9-10),** 848-849 (2011).
17. R. Caldecott, "Optimisation of a Motorised Momentum Exchange Tether as a Space Debris Sweeper", M.Eng. thesis, University of Sheffield, 2014.
18. D. N. S. Kamarulzaman, "Motorised Momentum Exchange Tether Scale Model", B.Eng. thesis, University of Sheffield, 2014.
19. A. N. Danilin et al, Computers and Structures **72**, 141-147 (1999).
20. E.M. Levin, Acta Astronautica **32 (5)**, 399-403 (1993).
21. J. P. Kirrane, "Design of a Motorised Momentum Exchange Tether Deployer," M.Eng. thesis, Aerospace Engineering, University of Sheffield, 2014.